https://doi.org/10.1016/j.soildyn.2020.106355

Manuscript Details

Manuscript number	SOILDYN_2020_490
Title	Partially Drained Cyclic Behaviour of Granular Fill Material in Triaxial Condition
Article type	Research Paper

Abstract

The dynamic responses of granular materials subjected to cyclic loading under partially drained condition were seldom investigated, though the partially drained condition is commonly existing for the granular materials that locate nearby the drainage boundaries. Besides, the prevalent studies mainly focus on the liquefaction behaviour of granular materials under high stress levels. In this study, a granular fill material was chosen as testing material. A series of partially drained cyclic triaxial tests was conducted with low level of cyclic loading and high cycle number that are commonly experienced in the geostructures of transportation projects. Note that the cyclic triaxial test under partially drained condition is a model test rather than an element test since the distribution of excess pore water pressure is not homogeneous inside the specimen. The test results show that cyclic loading induces the reconstruction effect on the microstructure of the specimen, thereby changing the trend between permeability and void ratio. Under partially drained condition, the granular fill material normally experiences a sudden decrease of stiffness and a quick increase in deformation during the first cycles of loading, followed by gradually decreasing excess pore water pressure and stabilizing deformation. Importantly, the deformation response of the material can be contributed by two items: (a) that caused by densification effect of applied cyclic loading and (b) that due to the dissipation of excess pore water pressure. Two linear relationships were established to correlate the deformations with excess pore water pressure and applied cyclic loading.

Keywords	cyclic triaxial tests, granular material, partially drained, excess pore water pressure, permanent strain

Corresponding Author	Wei-Qiang FENG
Corresponding Author's Institution	The Southern University of Science and Technology
Order of Authors	Wen-Bo CHEN, Kai Liu, Wei-Qiang FENG, Jianhua Yin
Suggested reviewers	Wan-Huan Zhou, Lin Guo, Guanlin YE, Dongsheng XU

Submission Files Included in this PDF

File Name [File Type]

HIghlight.docx [Highlights]

Partially drained cyclic test_text.docx [Manuscript File]

Partially drained cyclic test_figure.docx [Figure]

Partially drained cyclic test_table.docx [Table]

declaration-of-competing-interests 2020.docx [Conflict of Interest]

To view all the submission files, including those not included in the PDF, click on the manuscript title on your EVISE Homepage, then click 'Download zip file'.

Research Data Related to this Submission

There are no linked research data sets for this submission. The following reason is given:
Data will be made available on request

1. Partially drained cyclic tests with low stress and high cycle number was performed.
2. Effect of microstructure reconstruction on permeability of soil was revealed.
3. Resilient and permanent strain behavior were investigated.
4. Permanent strain was correlated with stress states by simple approach.

Partially Drained Cyclic Behaviour of Granular Fill Material in Triaxial Condition

by

Wen-Bo CHEN (Ph.D., Post-Doctoral Fellow)

Department of Civil and Environmental Engineering

The Hong Kong Polytechnic University, Hung Hom, Kowloon, Hong Kong, China

Email: geocwb@gmail.com

Kai LIU (Ph.D. Candidate)

Department of Civil and Environmental Engineering

The Hong Kong Polytechnic University, Hung Hom, Kowloon, Hong Kong, China

Email: kevin-kai.liu@connect.polyu.hk

Wei-Qiang FENG (Ph.D., Assistant Professor) (Corresponding Author)

Department of Ocean Sciences and Engineering,

The Southern University of Science and Technology, China.

Email: fengweiqiang2015@gmail.com

Jian-Hua YIN (Ph.D., Chair Professor)

Department of Civil and Environmental Engineering,

The Hong Kong Polytechnic University, Hung Hom, Kowloon, Hong Kong, China

Email: cejhyin@polyu.edu.hk

A manuscript submitted to *Soil Dynamics and Earthquake Engineering* for possible publication as a research paper

April 2020

ABSTRACT:

The dynamic responses of granular materials subjected to cyclic loading under partially drained condition were seldom investigated, though the partially drained condition is commonly existing for the granular materials that locate nearby the drainage boundaries. Besides, the prevalent studies mainly focus on the liquefaction behaviour of granular materials under high stress levels. In this study, a granular fill material was chosen as testing material. A series of partially drained cyclic triaxial tests was conducted with low level of cyclic loading and high cycle number that are commonly experienced in the geostructures of transportation projects. Note that the cyclic triaxial test under partially drained condition is a model test rather than an element test since the distribution of excess pore water pressure is not homogeneous inside the specimen. The test results show that cyclic loading induces the reconstruction effect on the microstructure of the specimen, thereby changing the trend between permeability and void ratio. Under partially drained condition, the granular fill material normally experiences a sudden decrease of stiffness and a quick increase in deformation during the first cycles of loading, followed by gradually decreasing excess pore water pressure and stabilizing deformation. Importantly, the deformation response of the material can be contributed by two items: (a) that caused by densification effect of applied cyclic loading and (b) that due to the dissipation of excess pore water pressure. Two linear relationships were established to correlate the deformations with excess pore water pressure and applied cyclic loading.

Keywords: cyclic triaxial tests, granular material, partially drained, excess pore water pressure, permanent strain.

1. Introduction

In the last several decades, significant progress has been advanced in understanding the rationales underlying the macroscopic responses of the saturated granular materials under cyclic loading. Most of the studies were conducted by implementing cyclic triaxial tests, in which the granular materials were compressed or extended under drained or undrained condition [1-11]. The granular materials are widely adopted as filling materials in transport infrastructures, such as pavement, ballasted and ballastless railways [9, 12-14]. One of the main functions of these granular materials is to provide drainage paths to drain the rainwater due to their relatively high permeability. Therefore, under the traffic loading, the granular materials are frequently serving in a partially drained condition, in which the build-up of excess pore water pressure and drainage of water in the granular materials occur simultaneously. The partially drained condition commonly exists in the granular materials that locate nearby the drainage boundaries, such as the surface of highway and railway embankment and the gravel or sand drains in the treated ground. Compared with the behaviour of granular materials under drained or undrained condition, their behaviour under partially drained condition is complexed by a coupling effect of a) decrease of effective confining pressure due to the increase of excess pore water pressure, and b) volumetric contraction due to the drainage of water. This coupling effect may further induce an excess settlement and a loss in bearing capacity, which will probably decrease the stability or even result in the failure of the geostructures.

Relative to the studies on granular materials, more studies, though not many, have been conducted on the cyclic behavior of cohesive soils under partially drained condition. Hyodo et al. [15] stated that the soft clay beneath nearshore or offshore structures and railway embankment are subjected to a long-term cyclic wave and traffic loadings, thereby inducing the alternate repetition between the generation and dissipation of excess pore pressure. A series of cyclic triaxial tests with the variation of cyclic deviator stress were conducted. They proposed a prediction model to describe the behaviour of clay in partially drained condition by calculating the excess pore water pressure based on the results of undrained cyclic triaxial tests combined with the theory of consolidation. Sakai et al. [16] implemented a series of cyclic triaxial tests on silty clay under drained and undrained conditions, then, modified and validated the model by Hyodo et al. [15] to incorporate the non-linear compressibility of soil. Indraratna et al. [17] conducted a series of large-scale cyclic triaxial tests on kaolinite clay with prefabricated vertical drain (PVD) installed in the center of the specimen under undrained and partially drained conditions. The results of tests indicate that PVD assists in the dissipation of excess pore water pressure in the specimen, the rate of which depends on the distance to the drain. However, the above-mentioned tests only investigated the effect of effective confining pressure and cyclic deviator stress on the behaviour of cohesive soil under partially drained condition.

Few attentions have been paid on the cyclic behaviour of granular materials under partially drained condition. After analyzing a group of cyclic undrained and partially drained triaxial tests on Toyoura sand, Yamamoto et al. [18] found that the initial liquefaction only occurs after reaching a certain limit of cyclic shear stress ratio (cyclic deviator stress over the double of effective confining pressure). Moreover, they concluded that permeability, drainage length, and loading frequency are three core factors that control the liquefaction potential of the sand under partially drained condition. A significant decrease in permeability of sand under dynamic compaction was observed by Chapuis et al. [19]. Mangal [20] highlighted the effect of dilatancy of sand on the build-up of excess pore water pressure in partially drained cyclic physical model test of shallow foundation.

Based on the above review, it can be seen that the existing studies about the cyclic behaviour of geomaterials under partially drained condition are limited to cohesive soil and clean sand with a narrow gradation. Furthermore, the above studies normally paid more attention to the cyclic strength of the geomaterials, particularly focusing on the critical shear stress ratio that induces the failure of cohesive soils and the liquefaction (cyclic mobility) of sand, in which the stress and strain levels are high. In contrast, for the granular material layers in transport infrastructure, firstly, the static and cyclic stress levels are normally much lower than the corresponding failure strength; secondly, the control limit of axial strain is strictly low; thirdly, a large number of cyclic loading will be experienced in the service life. Therefore, the cyclic behaviour of granular materials that are adopted as filling materials in transport infrastructures under partially drained condition is still an open question.

In this study, a poorly-graded coarse-grained soil is adopted as the testing material. A detailed characterization of soil at micro and macro scale was implemented and presented. Then, three static compression tests were conducted on the saturated specimens under drained condition. Subsequently, a series of cyclic triaxial tests on the saturated soil specimens under partially drained condition with variations of initial effective confining pressure ($\sigma_3^{'}$) , cyclic deviator stress (q_{cyc}), frequency (f), cycle number (N), and consolidation stress ratio ($\sigma_1^{'}/\sigma_3^{'}$). The changes of excess pore water pressure (Δu), resilient modulus (M_r), permanent volumetric and axial strains ($\Delta\varepsilon_v$ and $\Delta\varepsilon_a$), and the Poisson's ratio (υ) during cyclic loading tests will be presented and discussed. Several specimens subjected to cyclic loading were followed by drained static compression tests to evaluate the post-cyclic behaviour of the specimen. This investigation was aimed to provide a detailed database of experimental evidence of partially drained behaviour of granular fill materials in transport infrastructures.

2. Testing material, specimen preparation, apparatus and scheme

Testing material

The tested granular soil is a filling material, that is adopted in the high-filled embankment of an airport. The soil is classified as poorly-graded gravel with sand according to ASTM D 2487-06 [21]. Note that all particles larger than 20 mm in diameter were removed by sieving. Figure 1 shows the particle size distribution curve of the tested fill material after scaling. The scaled-down soil was first divided into eight groups characterized by eight particle size ranges: 10–20 mm, 5–10 mm, 2–5 mm, 0.3–2 mm, 0.212–0.3mm, 0.15–0.212 mm, 0.063–0.15mm, and <0.063 mm. For the soil specimens in characterization and triaxial tests, the predetermined mass of each group size was weighed and mixed together, according to the particle distribution curve as shown in Figure 1. The basic index values are listed in Table 1.

For better understanding the soil behaviour at the particle scale, microhardness of single particles was measured. Several particles from the size range of 2-5 mm were selected and cast by Epoxy to form a sliced specimen. Then, the sliced specimen was carefully polished by a grinding&polishing equipment (Buehler AutoMet 250) until the soil particles were clearly exposed to the air [22, 23, 24]. Figure 2(a) presents a typical microscopic view of the cross-section of a single soil particle. The soil particle comprises angular particles (bright areas) and the bonding materials (dim areas). The measurements were repeated for dry and saturated specimens. Figures 2(b) and 2(c) show the typical indentations on bright angular particles and bonding materials. As shown in Figure 3(a), when the soil particles are air-dried, the average Vickers microhardness (VM) of bright particles and bonding materials are 1387.1 kg/mm^2 and 66.5 kg/mm^2, respectively. Combined with the analysis of the content of oxide by X-ray fluorescence (XRF) test, as listed in Table 2, it is reasonable to conclude that the bright angular particles and bonding materials are quartz and clay minerals, respectively. Figure 3(b) shows that the VM values of bright particles and bonding materials will decrease to 1317.7 kg/mm^2, and 23.3 kg/mm^2, respectively, after saturation. The electron microscope scan of a typical particle is shown in Figure 4. It clearly shows that the particle is a clump of agglutinated materials, including angular particles and the attached small sheets. Therefore, it can be inferred that the compression of the specimen is accompanied by particle crushing due to the disaggregation of clay minerals under the effects of loading and soaking [25].

Specimen preparation

According to the particle size distribution curve shown in Figure 1, the oven-dried soil in predetermined mass from each size group was weighed and mixed together. Subsequently, the de-aired water was added into the soil to achieve the optimum water content. After mixing thoroughly, the soil was matured for at least 24 hrs. Then, the matured soil was compacted in a mold with an internal diameter of 100 mm using a rotary hammer in five layers. Each soil layer was compacted to achieve a height of 40 mm and a target dry density of 1.87 Mg/m^3 (88% of MDD). After finishing the compaction of each layer, the surface of the layers was scratched to ensure proper bonding with the subsequent soil layer.

Testing apparatus and scheme

An electro-hydraulically actuated servo-controlled loading apparatus (GCTS, USA) was utilized for the cyclic triaxial tests. For each triaxial specimen, as shown in Figure 5, two high-precision Linear Variable Differential Transformers (LVDTs) (RDP, UK) were attached at diametrically opposite sides of specimen for measuring the local vertical strain. For each specimen consolidated under an effective confining pressure of 100 kPa, a new LVDTs-based radial strain measurement device was attached at the middle height of the specimen. The new device is capable of measuring radial strain of specimen under both static and cyclic loadings. The details of this system are systematically introduced in Chen et al. [26]. With the results of radial strain, the Poisson's ratio can be calculated. The test scheme is listed in Table 3. Three levels of initial effective confining pressure (50, 100, 200 kPa) were selected in consolidation stage for static and cyclic triaxial tests. For three static compression tests, the specimens were sheared under drained condition. The effects of loading frequency and consolidation stress ratio are only investigated on the specimens consolidated under 100 kPa initial effective confining pressure. In the cyclic triaxial test, a series of stepwise-increased cyclic deviator stresses at an interval of 25 or 30 kPa was applied. The stress paths for cyclic tests are presented in Figure 6. Considering the control limit of axial strain in transport infrastructure is quite strict, especially for the pavement of airport and the embankment of railway, the stepwise-increased cyclic loadings were stopped after the accumulated (permanent) axial strain of the specimen reached 3 to 4 %. For each level of cyclic loading, 10000 loading cycles were applied. Note that post-cyclic compression was conducted in drained condition after the completion of cyclic loading for three specimens such that the post-cyclic strength and deformation behaviour can be evaluated. For the specimen consolidated under 200 kPa, the isotropic consolidation stress was increased step by step. The permeability tests were conducted after each stage of consolidation and cyclic loading to determine the relationship between void ratio and permeability.

To facilitate the saturation of specimens, all the specimens were flushed by Carbon Dioxide for 20 minutes. Then, the de-aired water was introduced from the bottom of the specimens to occupy the majority of voids in the specimen under the cell pressure of 25 kPa. Lastly, the back pressure saturation method was adopted to achieve a minimum B-value of 0.97. The typical changes of volumetric strain, axial strain and radial strain of one specimen during introducing water, which is also called collapse deformation, are presented in Figure 7. It can be seen that all the strains increase quickly at the beginning, then gradually tend to level off. Chen et al. [27] prepared the specimens with the same material and followed the same procedure. They stated that the matric suction of the specimens after compaction ranged from 20 kPa to 40 kPa and the air entry value on the drying path was 1.8 kPa. Therefore, the changes of strains can be inferred to be mainly induced by the release of matric suction. The strain levels showed in Figure 7 also indicate that the tested material is not prone to collapse under wetting.

Note that during cyclic loading, the drainage valve at the bottom of the specimen was kept open and excess pore water pressure of specimen was measured at the top of specimen. Therefore, the cyclic triaxial test resembles a model test rather than an element test since the distribution of excess pore water pressure is not homogeneous inside the specimen.

3. Test results and discussions

Hydraulic conductivity of tested granular fill material

For the specimen consolidated under 200 kPa, a series of stepwise-increased isotropic effective confining pressures (10 kPa, 20 kPa, 50 kPa, 100 kPa, 150 kPa, and 200 kPa) was applied. At each stage of loading, the vertical permeability of the specimen was measured after the completion of consolidation. Four levels of constant water head difference were maintained between the top and bottom of the specimen to determine the permeability at one stress state, then the average value of permeability was calculated. The corresponding void ratio was calculated based on the initial void ratio and the water volume draining out from the specimen under cyclic loadings. The same approach was applied to determine the permeability of the specimen after each stage of cyclic loading. Figure 8(a) shows the relationship between the permeability and void ratio under isotropic consolidation. The blanked circle dots represent the measured results and the solid fitting line shows that the logarithmic value of permeability decreases almost linearly with decreasing void ratio. Other five sets of data from literature are plotted in Figure 8(a) for comparison. It can be seen that the permeability level of the tested soil locates between that of uniformly-graded clean sand (silica sand or Toyoura sand) and the silt or silty sand, though the particles with diameter larger than 1 mm account for more than 50% in mass. This proves that the permeability is more dominated by the existence of the finer particles. For one specific soil, the void ratio plays a significant role in its drainage capacity, which inversely influences the compressibility of the soil, *i.e.* the change of void ratio.

As shown in Figure 8(b), an obvious sudden change occurs for the permeability after the lowest cyclic loading (25 kPa) is applied. Then the trend of permeability with void ratio differs greatly with that under multi-stage isotropic loading. It can be seen that the decreasing rate of permeability with the void ratio under cyclic loading increases compared to that under isotropic loading. This is possibly induced by the reconstruction effect from cyclic loading on the microstructure of specimen, which is presented by the increase of micro-pores and the decrease of macro-pores. The disaggregation of particles of the tested soil is aggravated under cyclic loading, leading to an increase in the percentage of fine particles and further resulting in the increase of micro-pores. It can be concluded that the change of particle size distribution curve (the crushing behavior of particles), except the change of void ratio, should be taken into account when investigating the hydraulic conductivity of one specific soil.

Static compression and post-cyclic strength

Figure 9 shows the stress-strain behaviour of the specimens with and without cyclic loading. For the specimens with cyclic loading, the deviator stress rose from zero point since the cyclic deviator stress was totally released before compression commenced. It can be seen that the initial modulus of post-cyclic compression curve is much higher than that of the specimen compressed under the same pressure without cyclic loading. Moreover, the strain level of the turning point, at which the deviator stress starts to level off, becomes smaller in the post-cyclic compression cases. Importantly, the maximum deviator stresses for the specimens consolidated under 50 kPa, 100 kPa and 200 kPa decreased by 15.5%, 9.6% and 13.9 %, respectively. This finding shows that the tested fill material degrades due to cyclic loading so that the design parameters for the embankment based on the conventional triaxial tests without cyclic loading are on the unsafe side. Therefore, the stability problem of the geostructure should take the effect of cyclic loading into consideration.

Excess pore water pressure

As mentioned in Section 2, the cyclic tests in this study resemble more a model test rather than an element test such that the pore water pressure distribution is not homogeneous throughout the specimen. Note that the build-up of excess pore water pressure corresponding to the cyclic loading is quite complex under partially drained condition. The profile of excess pore water pressure along the height of the specimen keeps varying from time to time depending on the stress level, loading frequency, void ratio, drainage path distance, and the change of particle size distribution. Based on the assumption adopted by Hyodo et al. [15], the pore water pressure measured at the top of the specimen can be reasonably regarded as the maximum one in the specimen due to its longest drainage path to the draining boundary, which is located at the bottom of the specimen. Figure 10 shows the build-up of excess pore water pressure of all specimens under cyclic loading. As the cyclic deviator stress is relatively small, the tests were all stopped before the liquefaction was triggered, i.e., the excess pore water pressure is equal to the initial effective confining pressure. It can be observed that the excess pore water pressure shoots up to a high level, then followed by a gradual decrease. Figure 10(a) shows the build-up of excess pore water pressure under different levels of confining pressure and the same loading frequency of 1 Hz. Unexpectedly, the maximum excess pore water pressure occurred when the specimen was consolidated under 50 kPa and subjected to a cyclic loading of 50 kPa. The transient high level of excess pore water pressure dropped down to a small level immediately. This dramatic change possibly resulted from the relatively high compressibility or high void ratio, which led to an instant volume contraction of the specimen. Then the high permeability enabled a quick dissipation of excess pore water pressure. If the excess pore water pressure is normalized by the initial effective confining pressure, it can be concluded that higher initial effective confining pressure increases the resistance to the build-up of excess pore water pressure. As shown in Figure 10(b), the higher loading frequency results in the higher maximum value of excess pore water pressure. With the increase of cyclic deviator stress, the specimens loaded under 0.25, 0.5 and 1 Hz showed a general decreasing trend of maximum pore water pressure. However, the specimen with cyclic loading of 2 Hz obtained its highest excess pore water pressure when the cyclic deviator stress of 130 kPa was applied, showing that the increasing frequency and cyclic stress level are two adverse factors in evaluating the liquefaction resistance or stability problem of the layer of fill materials in the embankment. For railway engineering projects, fortunately, the high-speed passenger trains normally exert low levels of dynamic stress on the subgrade, while heavy freight trains normally run at slow speed. On the contrary, it is necessary to consider the combined effects of high stress level and loading frequency for the embankment of the airport, which will experience the transient high level of dynamic stress of high frequency during the landing and take-off of the airplanes. Figure 10(c) shows that a slightly higher level of excess pore water pressure is reached for the specimens consolidated under a higher consolidation stress ratio. It can be speculated that this small difference is mainly due to the smaller void ratio, which represents the lower permeability.

Resilient modulus

Resilient modulus is defined as the ratio of the amplitude of cyclic deviator stress to the recoverable axial strain in one loading cycle. It is a fundamental parameter to describe the stiffness of soil under cyclic loading and commonly adopted for characterizing the compacted fill materials in substructures of pavement or railway [12, 14]. Figure 11 presents the variation of M_r with increasing cycle number under different stress states. As can be observed in Figure 11(a), with the same loading frequency of 1 Hz, M_r generally becomes larger under higher confining pressure, which confirms with the findings by the majority of studies [*e.g.* 30, 31]. It can also be noted that the cyclic deviator stress is less influencing to M_r compared to the confining pressure for this specific granular fill material. When a higher level of cyclic loading is applied, M_r shows a sudden decrease in the first several loading cycles, then followed by a gradual increase until a stable state is achieved. The sudden decrease is most significant for the specimen under the confining pressure of 50 kPa. This is in accordance with the trend of the build-up of excess pore water pressure, which decreases the effective confining pressure sustained by soil skeleton, thereby facilitating the interparticle slip and skeleton deformation. After the dissipation of excess pore water pressure, the soil specimen regains stiffness due to the increase of effective confining pressure. This indicates that the granular fill material at the top part of the subgrade is prone to fail at low effective confining pressure. Furthermore, with the development of rutting and the possible particle suffusion in gap-graded granular materials, the effective confining pressure will decrease further due to the drop of bulk density or unit weight. When coupling with saturated condition, the stability problem of the surface part will be fatal to the serviceability of the whole embankment. As for the effect of consolidation stress, it shows a slight strengthening effect on the resilient modulus when the cyclic deviator stress is relatively small (from 20 to 100 kPa), as shown in Figure 11(c). The higher consolidation stress would lead to a more densely contacted soil particle structure, in which the average area of each contact point is increased, and the macroscopic compressibility of the soil specimen is decreased. The increasing cyclic deviator stress gradually diminishes this strengthening effect. Therefore, for some typical practical projects, e.g. ballastless High-speed Railway, with the dynamic stress transferred from concrete slab to the embankment smaller than 20 kPa [32, 33], the resilient modulus tests on the specimens under anisotropic consolidation are inevitable, which, however, is normally overlooked in the prevalent standards, e.g. EN 13286-7 [34] and AASHTO T307-99 [35].

Poisson's ratio

In this study, the radial strain measurement system was only utilized for the specimens consolidated under 100 kPa. The corresponding values of Poisson's ratio were calculated and presented in Figure 12. It is challenging to measure accurately the radial strain change during each cycle of loading [26], thus some slight fluctuations can be observed in the figure. Generally, the Poisson's ratio increases with increasing cyclic deviator stress. Under higher loading frequency, the Poisson's ratio generally becomes larger. In contrast, the higher consolidation stress ratio induces a lower value of Poisson's ratio.

Accumulated axial and volumetric strains

The accumulated strain is defined as the sum of the irrecoverable strain occurs during each cycle of loading. Estimating the accumulated strain of granular materials in embankment subjected to cyclic loading is a major challenge for transport engineering projects. The control limits of the settlement after construction are very strict for the embankment of High-speed Railway (<15mm) or the embankment of airport (<50mm). Also, the strain levels of differential settlement should be strictly lower than 0.1-0.15% for the embankment of airport and 0.15-0.45% for High-speed Railway. However, accumulated strain behavior is less investigated compared to that of resilient modulus as it needs a larger number of specimens and much more time and effort. To the knowledge of authors, the accumulated strains (axial and volumetric strains) of granular fill materials under long-term cyclic loading and partially drained condition has never been investigated. As shown in Figure 13(a), the rising effective confining pressure increases the deformation resistance of the specimen. Figure 13(b) presents the effect of loading frequency on the development of accumulated axial strain. Generally, the specimens experienced higher accumulated axial strain when the loading frequency was higher. The accumulated axial strain normally increased quickly in the first cycles, followed by a stable state. Excessive deformation occurred for the specimen subjected to a 2 Hz cyclic loading when cyclic deviator stress reached 130 kPa. Figure 13(c) shows that the accumulated axial strain becomes larger with increasing consolidation stress ratio under each level of cyclic deviator stress. Therefore, the simplification of using isotropic confining pressure for permanent strain in EN 13286-7 [34] may underestimate the real strain level in the field, where the embankment is normally subjected to an anisotropic stress condition with larger vertical stress and lower lateral stress.

Figure 14 presents the relationship between the maximum mean stress ($P_{\max}$) under each level of cyclic deviator stress and the change of void ratio. To ease the comparison, the confining pressure for the calculation of maximum mean stress adopts the initial effective confining pressure before applying cyclic loadings. The maximum mean stress is reached when the cyclic deviator stress increases to its peak. On the other hand, the void ratio in the figure is a stable value at the end of each stage of loading. A reference curve, as shown in Figure 14, is composed of the mean effective stresses under different stages of isotropic confining pressure and the corresponding void ratios. The void ratio decreases at an obviously higher rate under cyclic loading, which is called the densification effect of cyclic loading, compared to that under isotropic loading. Specifically, the changes of the void ratio of the specimens under 100 kPa initial effective confining pressure are presented in Figure 15. The compression index, C_c, is calculated as:

$$C_c = -\Delta e / \Delta \log(p_{\max}) \tag{1}$$

The compression index for each specimen is also listed in Figure 15. The trends of C_c for different frequencies and stress ratios are identical to those of permanent strain with a larger value under higher frequency and higher consolidation stress ratio. A largest value of the compression index was achieved by the specimen under 2 Hz cyclic loading.

According to the simplification by Hyodo et al. [15] and Sakai et al. [16], the total volume change $\Delta\varepsilon_v$ can be expressed by:

$$\Delta\varepsilon_v = \Delta\varepsilon_{vu} + \Delta\varepsilon_{vl} \tag{2}$$

where $\Delta\varepsilon_{vu}$ is the volumetric strain resulted from the dissipation of excess pore water pressure, $\Delta\varepsilon_{vl}$ is the volumetric strain due to the densification effect of applied cyclic loading. As mentioned in Section 2, the cyclic triaxial test in this study is a model test, which has a clear boundary condition. Also, the excess pore water pressure distribution is inhomogeneous throughout the specimen with the largest exists at the impermeable boundary, i.e. the top of the specimen, and the lowest (can be regarded as zero) exists at the drainage boundary, i.e. the bottom of the specimen. Hyoto et al. [15] proved that except in the vicinity of the drainage boundary the excess pore water pressure rises up with the cycle number until reaching the peak value at which the contour of excess pore water pressure is of a trapezoidal shape. Then, the excess pore water pressure dissipates while keeping a parabolic shape until reaching a marginal level. Therefore, it is reasonable to assume that the equivalent average excess pore water pressure, Δu_a, throughout the specimen can be calculated as the two-thirds of the maximum excess pore water pressure measured at the top of the specimen, as expressed by:

$$\Delta u_a = \frac{2}{3}\Delta u_{\max} \tag{3}$$

This is also a common approach to estimate the average excess pore water pressure in a clay specimen with one permeable boundary and one impermeable boundary under 1D straining condition [36, 37]. Therefore, $\Delta\varepsilon_{vu}$ can be calculated as:

$$\Delta\varepsilon_{vu} = \Delta u_a \cdot m_v = \Delta u_a \cdot [\Delta e/(1+e_0)]/\Delta p_{\max} \tag{4}$$

where m_v is the coefficient of volume compressibility, e_0 is the initial void ratio and Δe is the change of void ratio. Note that m_v is a highly stress-path dependent parameter [38, 39]. On one hand, the Δu_a is bulk stress such that the corresponding m_v cannot be determined by the cyclic tests with varying deviator stress. On the other hand, no isotropic loading was applied after each stage of cyclic loading, in this study, to determine the m_v. Thus, the m_v corresponding to Δu_a was estimated based on the compression index of the normal compression line (NCL), which is shown in Figure 14 assuming that after the cyclic loading the void ratio of the specimen subjected to an isotropic loading will develop along a line that is parallel to the NCL. As shown in Figure 16, the relationship between $\Delta\varepsilon_{vu}$ and $\Delta u_{\max} / p_{\max}$ is plotted and a good linear relationship can be shown as:

$$\Delta\varepsilon_{vu} = 0.0328 \cdot \Delta u_{\max} / p_{\max} \tag{5}$$

Then, $\Delta\varepsilon_{vl}$ can be easily calculated using Eq. (2), and, as shown in Figure 17, it can be well correlated with q_{max}/p_{max} as a linear formula:

$$\Delta\varepsilon_{vl} = 0.0388 \cdot q_{max}/p_{max} \tag{6}$$

where q_{max} is defined as the maximum deviator stress can be achieved during cyclic loading. It can be seen that, irrespective of the confining pressure, loading frequency, and consolidation stress ratio, the volumetric strain due to the densification of cyclic loading has a unique linear relationship with q_{max}/p_{max}, with a standard error less than ±15%, which indicates that the volumetric strain due to the densification of cyclic loading under partially drained condition can be easily estimated by the test results from one drained cyclic test with multi-stage cyclic deviator stress.

4. Discussions of this study

In this study, the length of the drainage path (sample height) was kept constant for all the specimens. Also, the drainage direction in the field would be quite different from the condition in the triaxial test, where the drainage is only one-dimensional. Note that the permeability after cyclic loading was only measured for one specimen such that no generalized relationship between permeability and peak excess pore water pressure ratio as well as stress states can be established, which will be the main research focus in the future. The research findings in this study are valid for the specific ranges of loading conditions, including the confining pressure, frequency, consolidation stress ratio and cyclic deviator stress, which aims to simulate the stress conditions that are normally confronted in the transportation geostructures. Importantly, as a common limitation for most laboratory studies, the scale of the model test (triaxial specimen) may not be comparable to the actual dimensions of most practical problems.

5. Conclusions

In this study, a series of static and cyclic triaxial tests was implemented to focus on the dynamic responses of a granular fill material under partially drained condition, in which the top of the specimen was impermeable, and the bottom of the specimen was connected to a pressure controller that maintained the water pressure and allowed water drain freely. Due to the fact that the excess pore water pressure distribution inside the specimen subjected to cyclic loading is inhomogeneous, the cyclic triaxial test is a model test rather than an element test. Aim to simulate the condition that a granular fill material in a transport geostructure normally experiences, the specimens were subjected to multi-stage cyclic deviator stress with low stress level and high cycle number, instead of the investigation on liquefaction phenomenon under high stress levels, which has been widely reported in extensive studies. Based on the principal findings of the current results, the following conclusions can be drawn:

1. The permeability of granular fill material is more dominated by the existence of fine particles. Under isotropic loading, the logarithmic value of permeability decreases almost linearly with decreasing void ratio. After the cyclic loading is applied, however, the permeability decreases at an obviously higher rate with the decreasing void ratio. This is possibly induced by the reconstruction effect from cyclic loading on the microstructure of the specimen.
2. The stress-strain behaviour of the post-cyclic specimens shows a significantly higher initial modulus but lower shear strength compared to that of the specimens without subjected to cyclic loading.
3. The development of excess pore water pressure results from the dynamic disequilibrium between the contraction of the specimen and its drainage ability. Under partially drained condition, the excess pore water pressure normally increases dramatically to a high level, then followed by a gradual decrease. The increasing frequency and cyclic stress levels are two adverse factors to the deformation or stability of granular fill layers in the embankment.
4. Under partially drained condition, the granular fill material normally experiences a sudden decrease of stiffness and a quick increase in deformation at the first cycles of loading. The deformation response of the material can be reasonably divided into that caused by densification effect of applied cyclic loading and that due to the dissipation of excess pore water pressure. Two linear relationships were established to correlate the permanent deformations with excess pore water pressure and applied cyclic loading.

Credit Author Statement

Dr CHEN Wen-Bo: Data curation; Formal analysis; Investigation; Methodology; Validation; Roles/Writing – original draft;

Mr LIU Kai: Data curation; Methodology; Validation;

Dr FENG Wei-Qiang: Conceptualization; Formal analysis; Writing – review & editing.

Professor YIN Jian-Hua: Funding acquisition; Project administration; Supervision;

Acknowledgement

The work in this paper is supported by a Research Impact Fund (RIF) project (R5037-18), and three General Research Fund (GRF) projects (PolyU 152796/16E, PolyU 152209/17E; PolyU 152179/18E) from Research Grants Council (RGC) of Hong Kong Special Administrative Region Government of China. The authors also acknowledge supports from Research Institute for Sustainable Urban Development, Research Centre for Urban Hazards Mitigation, and three grants (BBAG, ZDBS, ZVNC) of The Hong Kong Polytechnic University.

References

[1] Seed HB, Idriss IM. Simplified procedure for evaluating soil liquefaction potential. J Soil Mech Found Div 1971;97(9):1249-1273.

[2] Ishihara K, Towhata I. Sand response to cyclic rotation of principal stress directions as induced by wave loads. Soils Found 1983;23(4):11-26.

[3] Indraratna B, Lackenby J, Christie D. Effect of confining pressure on the degradation of ballast under cyclic loading. Géotechnique 2005;55(4):325-328.

[4] Yang ZX, Li XS, Yang J. Undrained anisotropy and rotational shear in granular soil. Géotechnique, 2007;57(4):371-384.

[5] Wichtmann T, Niemunis A, Triantafyllidis T. On the determination of a set of material constants for a high-cycle accumulation model for non-cohesive soils. Int J Numer Anal Methods Geomech 2010:34(4):409-440.

[6] Ishikawa T, Sekine E, Miura S. Cyclic deformation of granular material subjected to moving-wheel loads. Can Geotech J 2011;48(5):691-703.

[7] Cao Z, Chen J, Cai Y, Gu C, Wang J. Effects of moisture content on the cyclic behavior of crushed tuff aggregates by large-scale tri-axial test. Soil Dyn Earthq Eng 2017;95:1-8.

[8] Chen WB, Yin JH, Feng WQ, Borana L, Chen RP. Accumulated permanent axial strain of a subgrade fill under cyclic high-speed railway loading. Int J Geomech 2018;18(5):04018018. DOI: 10.1061/(ASCE)GM.1943-5622.0001119

[9] Chen WB, Feng WQ, Yin JH, Borana L, Chen RP. Characterization of permanent axial strain of granular materials subjected to cyclic loading based on shakedown theory. Constr Build Mater 2019;198:751-761. DOI: 10.1016/j.conbuildmat.2018.12.012

[10] Xiong H, Yin ZY, Nicot F. A multiscale work- analysis approach for geotechnical structures. Int J Numer Anal Methods Geomech 2019;43(6):1230-1250.

[11] Shi XS, Nie J, Zhao JD, Gao Y. A homogenization equation for the small strain stiffness of gap-graded granular materials. Comput Geotech 2019;121:103440. DOI:10.1016/j.compgeo.2020.103440.

[12] Wang HL, Cui YJ, Lamas-Lopez F, Dupla JC, Canou J, Calon N, Saussine G, Aimedieu

P, Chen RP. Effects of inclusion contents on resilient modulus and damping ratio of unsaturated track-bed materials. Can Geotech J 2017;54(12):1672-1681.

[13] Wang HL, Chen RP, Qi S, Cheng W, Cui YJ. Long-term Performance of Pile-supported Ballastless Track-bed at various water Levels. J Geotech Geoenviron 2018;144(6): 04018035.

[14] Chen WB, Feng WQ, Yin JH. Effects of water content on resilient modulus of a granular material with high fines content. Constr Build Mater 2020;236:117542.

[15] Hyodo M, Yasuhara K, Hirao K. Prediction of clay behaviour in undrained and partially drained cyclic triaxial tests. Soils Found 1992;32(4):117-127.

[16] Sakai A, Samang L, Miura N. Partially-drained cyclic behavior and its application to the settlement of a low embankment road on silty-clay. Soils Found 2003;43(1):33-46.

[17] Indraratna B, Attya A, Rujikiatkamjorn C. Experimental investigation on effectiveness of a vertical drain under cyclic loads. J Geotech Geoenviron 2009;135(6):835-839.

[18] Yamamoto Y, Hyodo M, Orense RP. Liquefaction resistance of sandy soils under partially drained condition. J Geotech Geoenviron 2009;135(8):1032-1043.

[19] Chapuis RP, Gill DE, Baass K. Laboratory permeability tests on sand: influence of the compaction method on anisotropy. Can Geotech J 1991;26(4):614-622.

[20] Mangal JK. Partially-drained loading of shallow foundations on sand (Doctoral dissertation, University of Oxford) 1999.

[21] ASTM D 2487-06 Standard practice for classification of soils for engineering purposes (Unified Soil Classification System). Annual Book of ASTM Standards, ASTM International, West Conshohocken, PA. 2006

[22] Xuan DX, Zhan BJ, Poon CS. Assessment of mechanical properties of concrete incorporating carbonated recycled concrete aggregates. Cement Concrete Comp 2016;65:67-74.

[23] Zhan BJ, Xuan DX, Poon CS. Enhancement of recycled aggregate properties by accelerated CO_2 curing coupled with limewater soaking process. Cement Concrete Comp 2018;89:230-237.

[24] Cao S, Yilmaz E, Xue G, Yilmaz E, Song W. Loading rate effect on uniaxial compressive strength behavior and acoustic emission properties of cemented tailings backfill. Constr Build Mater, 2019, 213: 313-324.

[25] Chen WB, Liu K, Yin ZY, Yin JH. Crushing and Flooding Effects on One-Dimensional Time-Dependent Behaviors of a Granular Soil. Int J Geomech 2020;20(2):04019156.

[26] Chen WB, Feng WQ, Yin JH, Borana L. LVDTs-based Radial Strain Measurement System for Static and Cyclic Behavior of Geomaterials. Measurement 2020:107526.

[27] Chen WB, Liu K, Feng WQ, Borana L, Yin JH. Influence of matric suction on nonlinear time-dependent compression behavior of a granular fill material. Acta Geotech 2020;15:615-633.

[28] Lambe TW, Whitman RV. Soil mechanics 1969 553 pp.

[29] Lourenço SD, Wang G, Sassa K, Fukuoka H. Volumetric behavior of saturated sands under poor drainage conditions. J Geophys Res-Earth 2006 111(F3).

[30] Hicks RG, Monismith CL. Factors influencing the resilient properties of granular materials. High Res Rec 1971;345:15-31.

[31] Lekarp F, Isacsson U, Dawson A. State of the art. I: Resilient response of unbound aggregates. J Transp Eng 2000;126:66-75.

[32] Guo JH. Study on dynamic response of granular type A and type B fillings of high-speed railway. Soil Engrg. and Found 2012;26(10):116-120. (in Chinese)

[33] Qu CZ, Wang YH, Wei LM, Guo ZG. In-situ test and analysis of vibration of subgrade for Wuhan-Guangzhou High-Speed Railway. Rock and Soil Mech 2012;33(5):1451-1461. (in Chinese)

[34] CEN-European Committee for Standardization Unbound and hydraulically bound mixtures - Part 7: Cyclic load triaxial test for unbound mixtures. Brussels: European Standard. EN 13286-7. 2004.

[35] AASHTO. Standard method of test for determining the resilient modulus of soils and aggregate material. AASHTO T307, Washington. D.C. VA. 2007.

[36] Cheng CM, Yin JH. Strain-Rate Dependent Stress-Strain Behavior of Undisturbed Hong

Kong Marine Deposits under Oedometric and Triaxial Stress States. Mar Georesources Geotechnol 2005;23(1-2):61-92.

[37] Yin JH, Cheng CM. Comparison of strain-rate dependent stress-strain behavior from K_0-consolidated compression and extension tests on natural Hong Kong marine deposits. Mar Georesources Geotechnol 2006;24(2):119-147.

[38] Feng WQ, Yin JH. A new simplified hypothesis B method for calculating settlements of double soil layers exhibiting creep. Int J Numer Anal Met 2017;41(6):899-917.

[39] Yin JH, Feng WQ. A new simplified method and its verification for calculation of consolidation settlement of a clayey soil with creep, Can Geotech J 2017; 54(3):333-347.

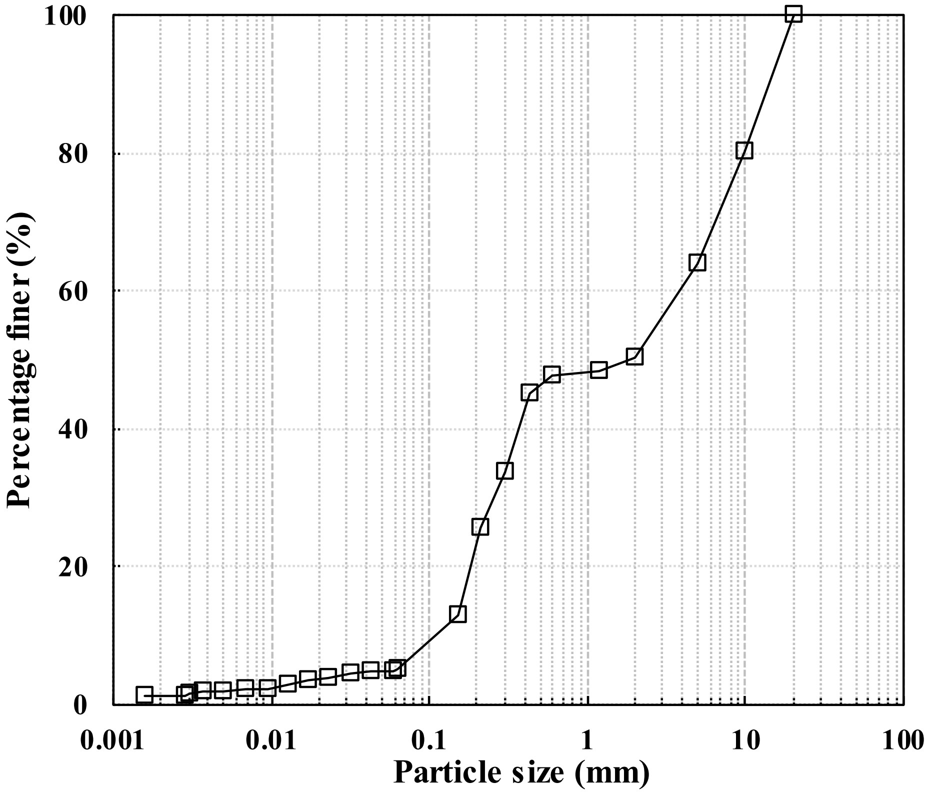

Figure 1. Particle size distribution curve of the granular fill material

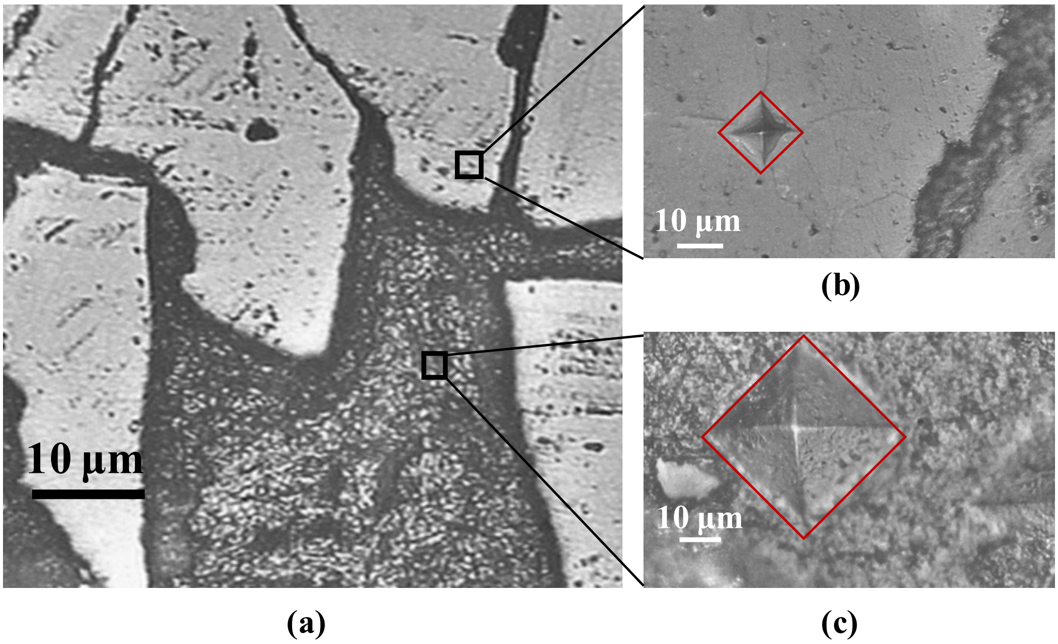

Figure 2. The microscopic view of (a) the cross-section of a single soil particle, (b) typical indentation point on an angular particle, and (c) typical indentation point on the bonding materials

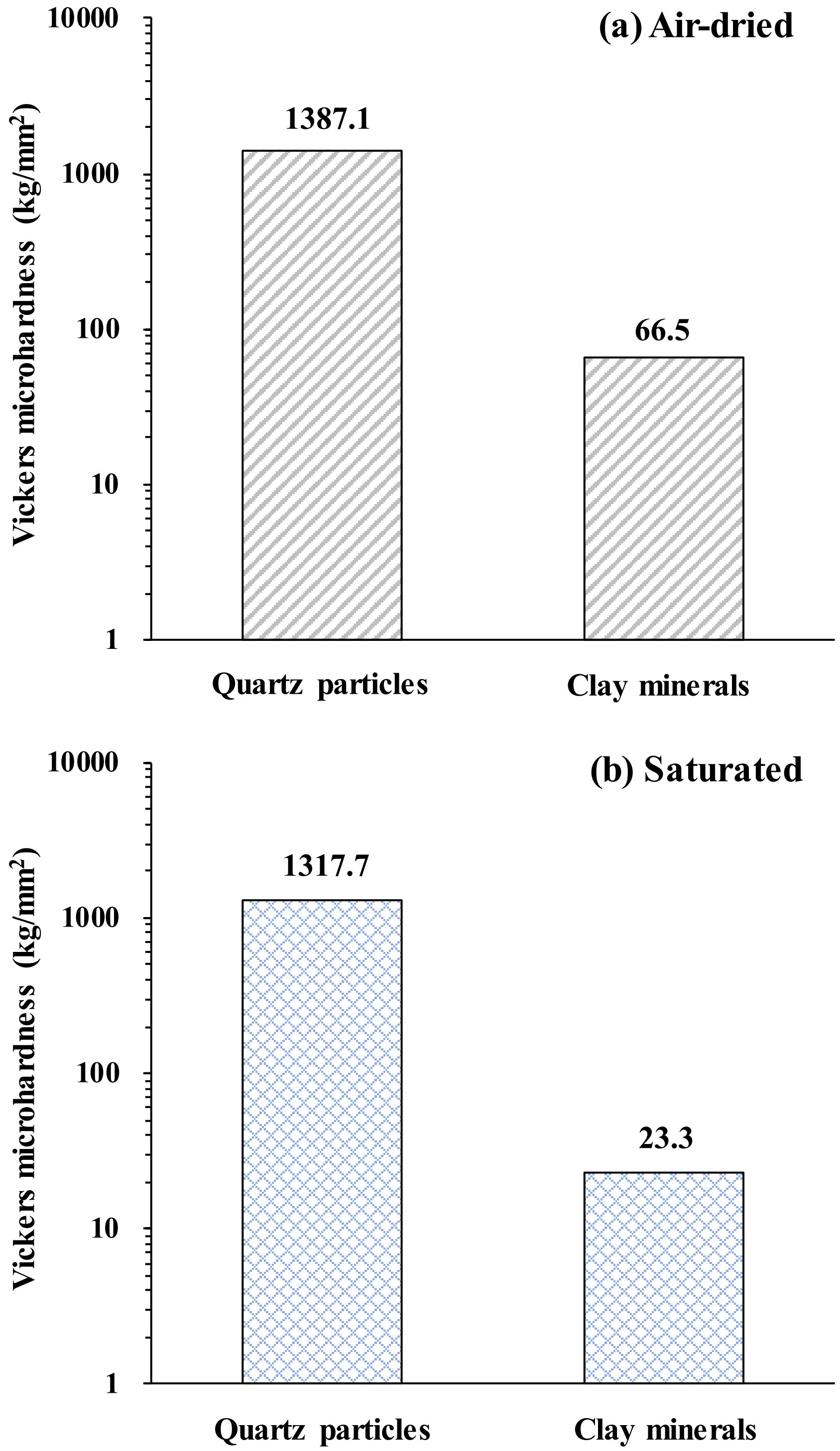

Figure 3. The Vickers microhardness of different positions on particles in (a) air dried and (b) saturated conditions

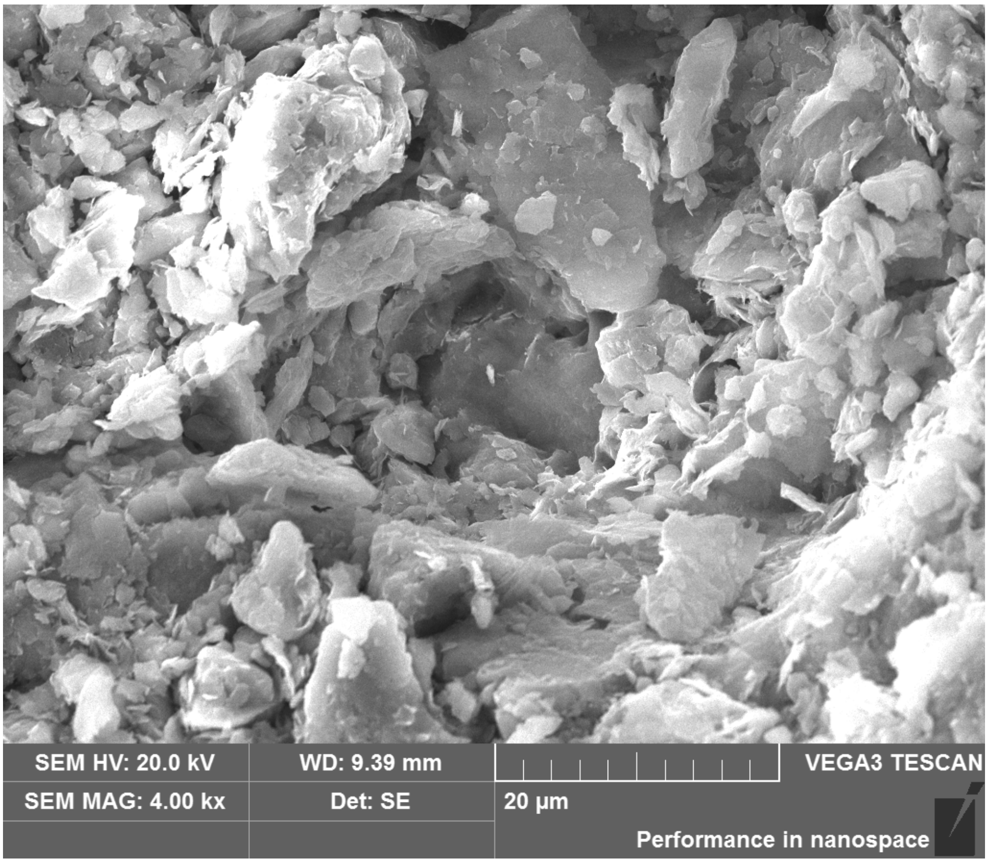

Figure 4. Electron microscope scan image of a typical particle of the granular fill material

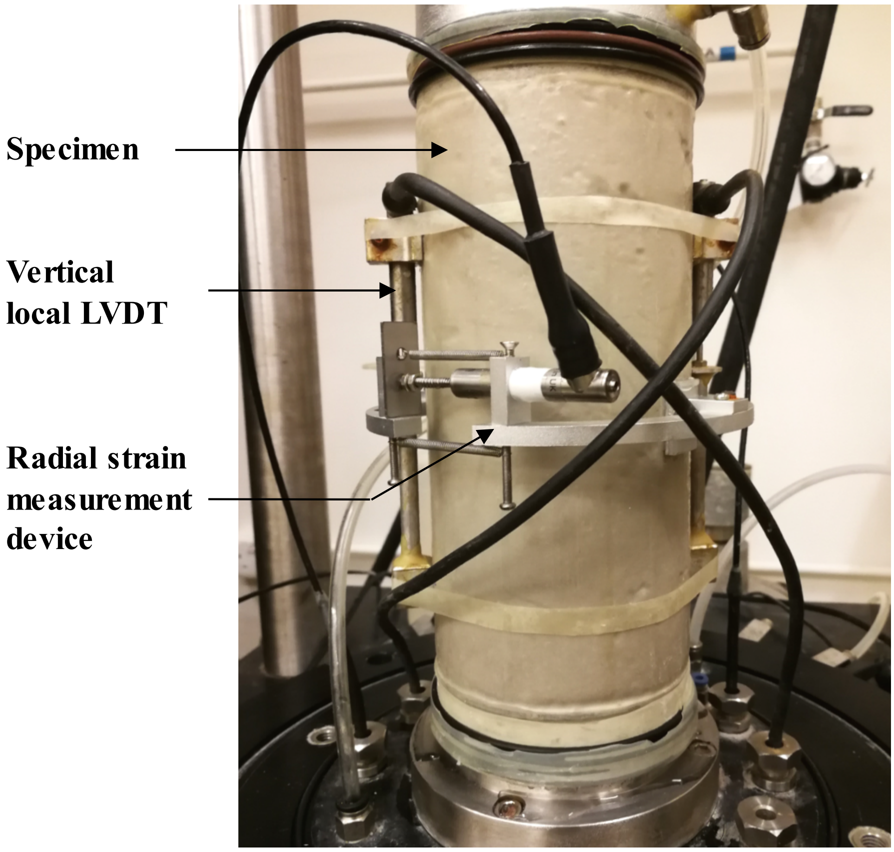

Figure 5. The setup of the on-specimen transducers for measuring vertical and radial strains of the specimen

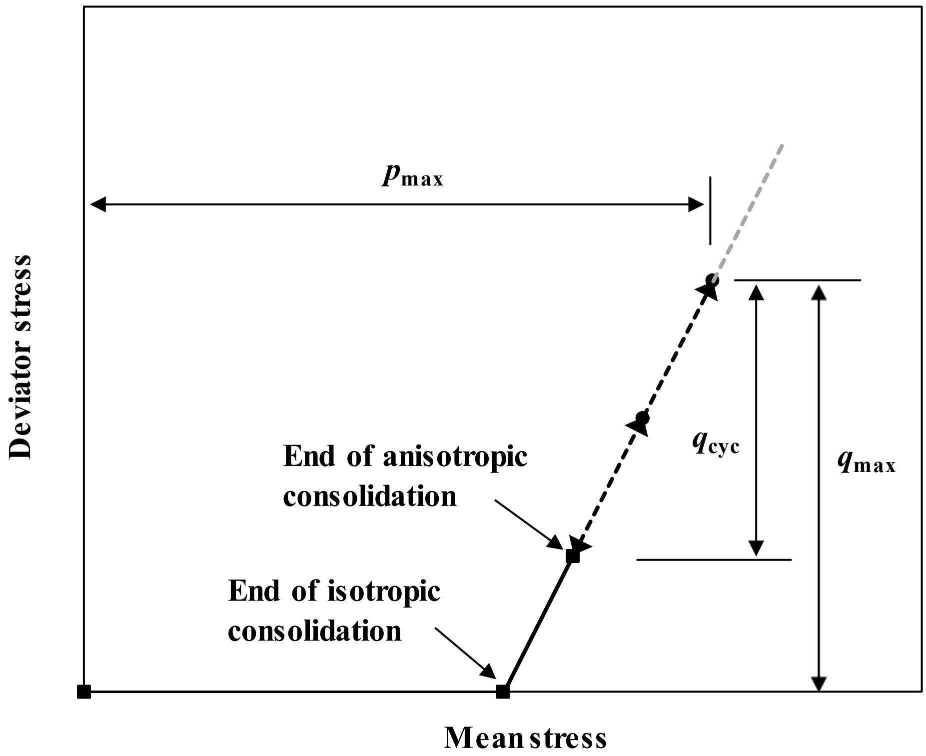

Figure 6. Illustration of stress paths for cyclic tests

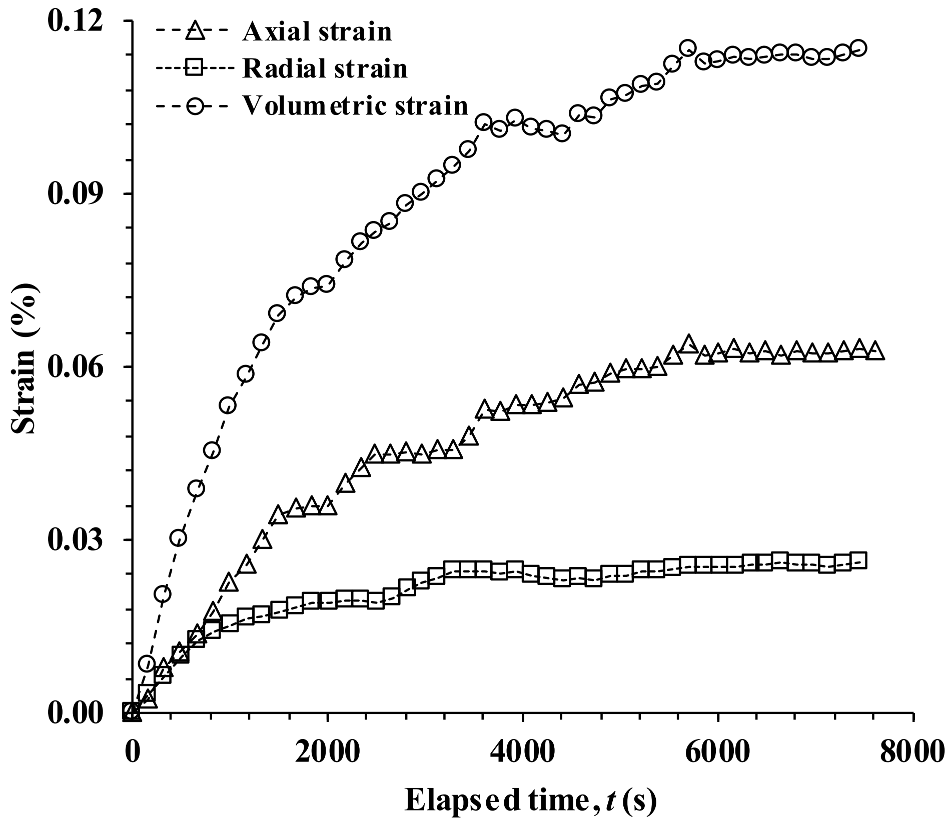

Figure 7. The typical changes of axial strain, radial strain, and volumetric strain of one specimen when introducing water into specimen during saturation stage

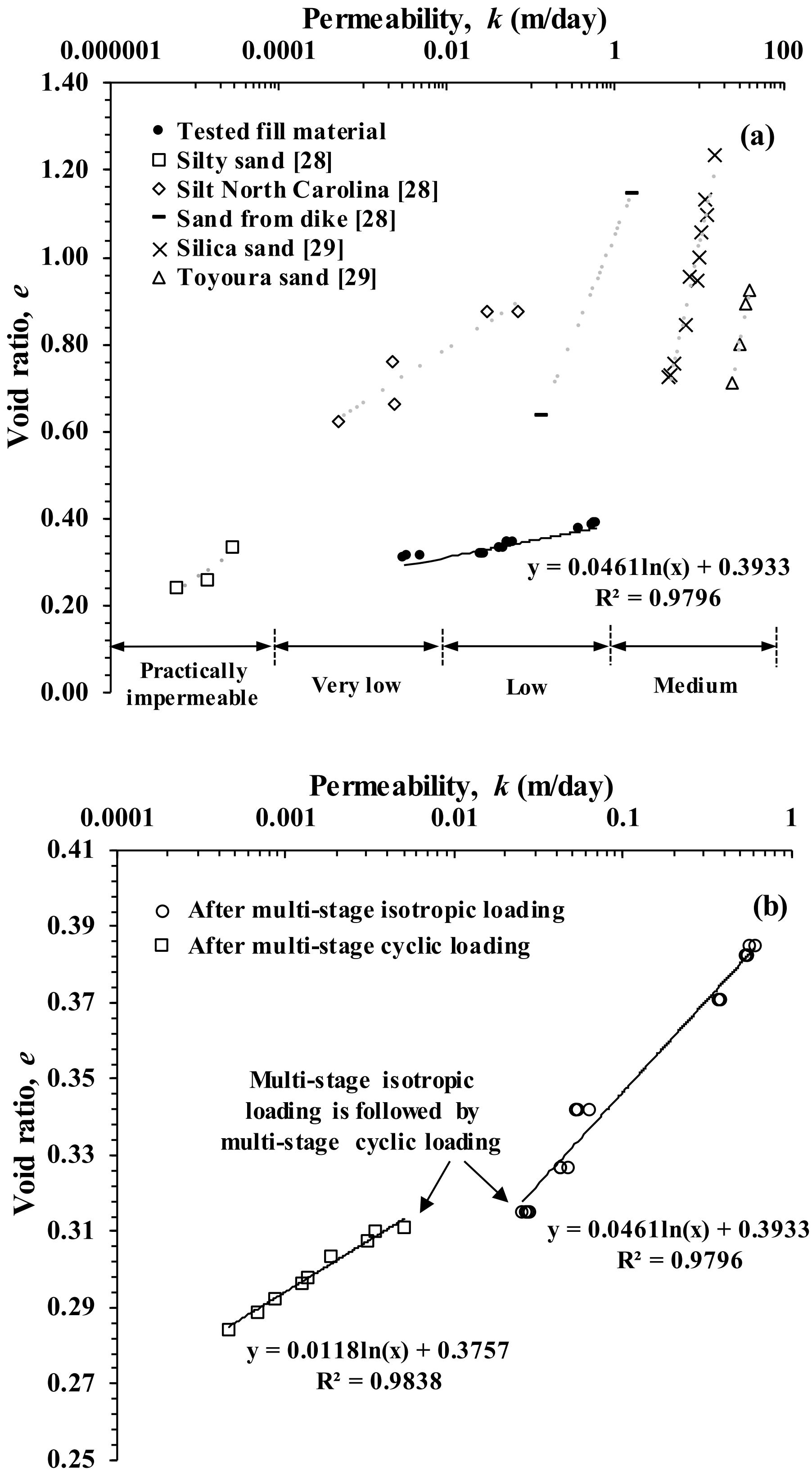

Figure 8. The relationships between permeability and void ratio (a) under multi-stage isotropic consolidation stress, and (b) after applying multi-stage cyclic loading

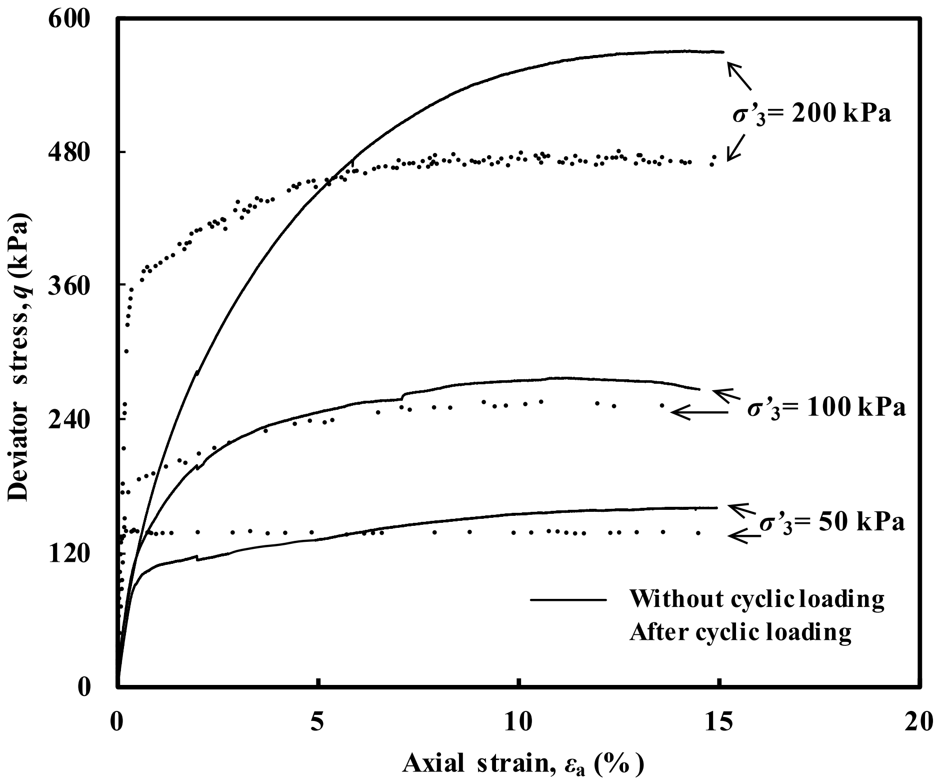

Figure 9. The stress-strain behaviour of the specimens after and without cyclic loading

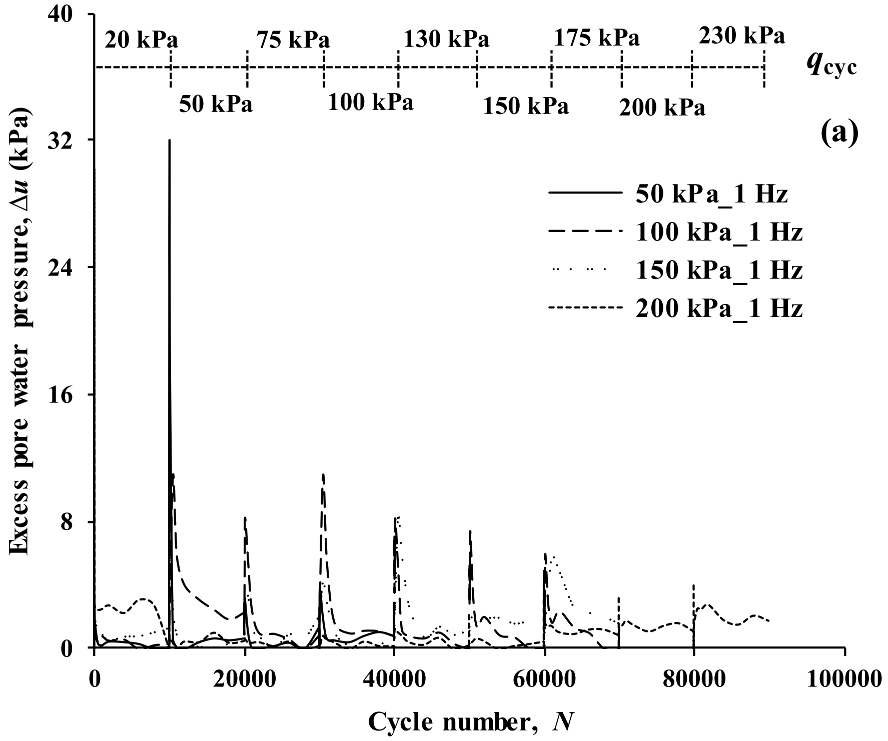

20 kPa
50 kPa
75 kPa
100 kPa
130 kPa
150 kPa
175 kPa
200 kPa
230 kPa
q_{cyc}
(a)
50 kPa_1 Hz
100 kPa_1 Hz
150 kPa_1 Hz
200 kPa_1 Hz
Excess pore water pressure, Δu (kPa)
Cycle number, N

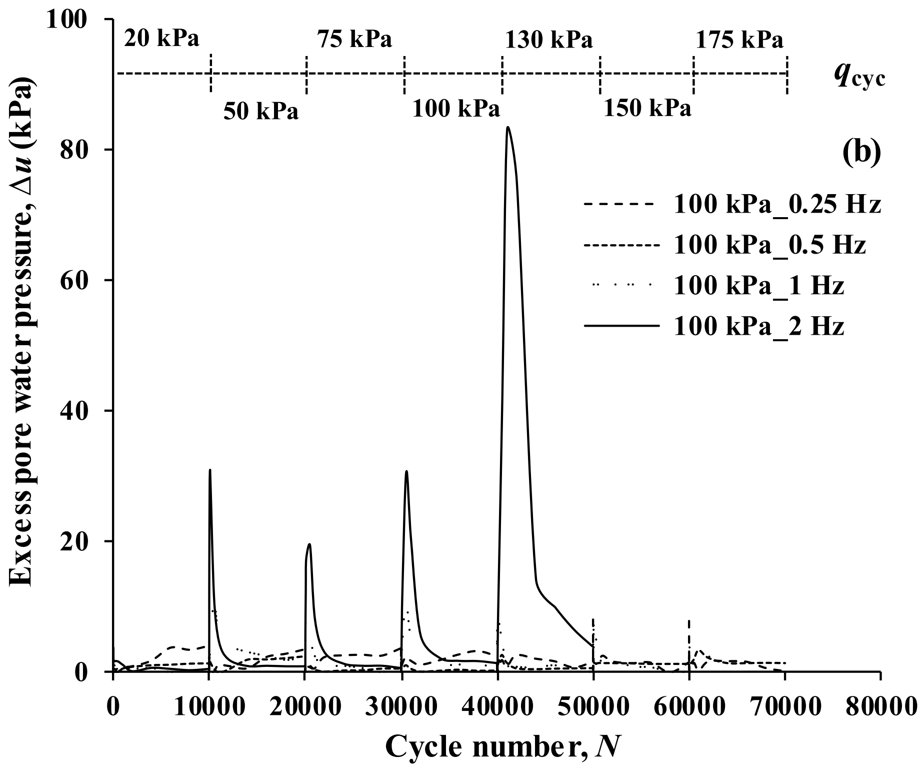

20 kPa
50 kPa
75 kPa
100 kPa
130 kPa
150 kPa
175 kPa
q_{cyc}
(b)
100 kPa_0.25 Hz
100 kPa_0.5 Hz
100 kPa_1 Hz
100 kPa_2 Hz
Excess pore water pressure, Δu (kPa)
Cycle number, N

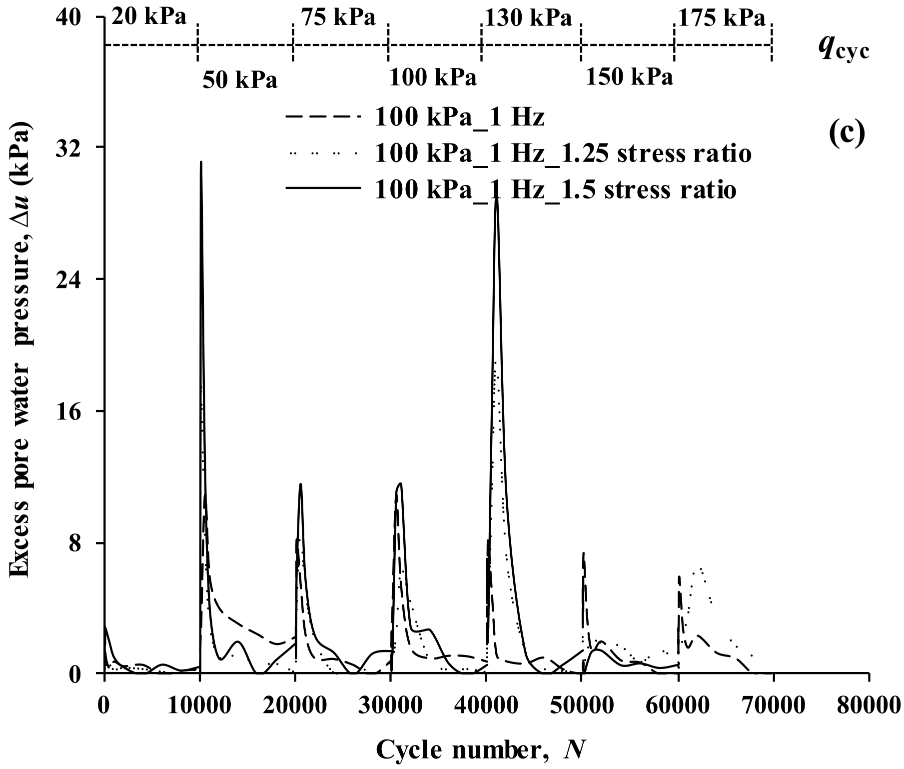

Figure 10. The plots of excess pore water pressure responses of the specimens subjected to cyclic loading *versus* cycle number under (a) different initial effective confining pressures, (b) different frequencies, and (c) different consolidation stress ratios

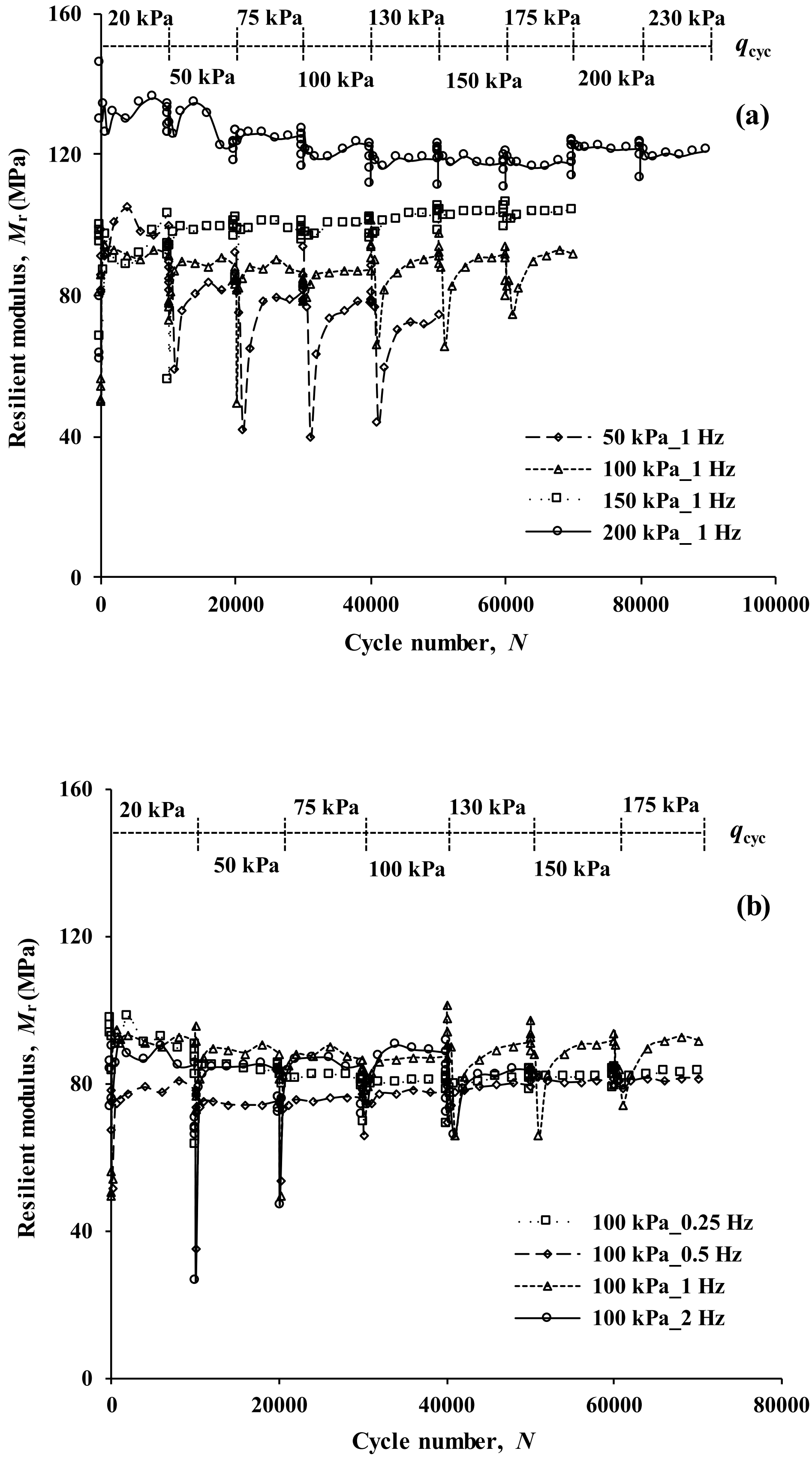
(a)
20 kPa
50 kPa
75 kPa
100 kPa
130 kPa
150 kPa
175 kPa
200 kPa
230 kPa
q_{cyc}
Resilient modulus, M_r (MPa)
Cycle number, N
50 kPa_1 Hz
100 kPa_1 Hz
150 kPa_1 Hz
200 kPa_ 1 Hz
(b)
20 kPa
50 kPa
75 kPa
100 kPa
130 kPa
150 kPa
175 kPa
q_{cyc}
Resilient modulus, M_r (MPa)
Cycle number, N
100 kPa_0.25 Hz
100 kPa_0.5 Hz
100 kPa_1 Hz
100 kPa_2 Hz

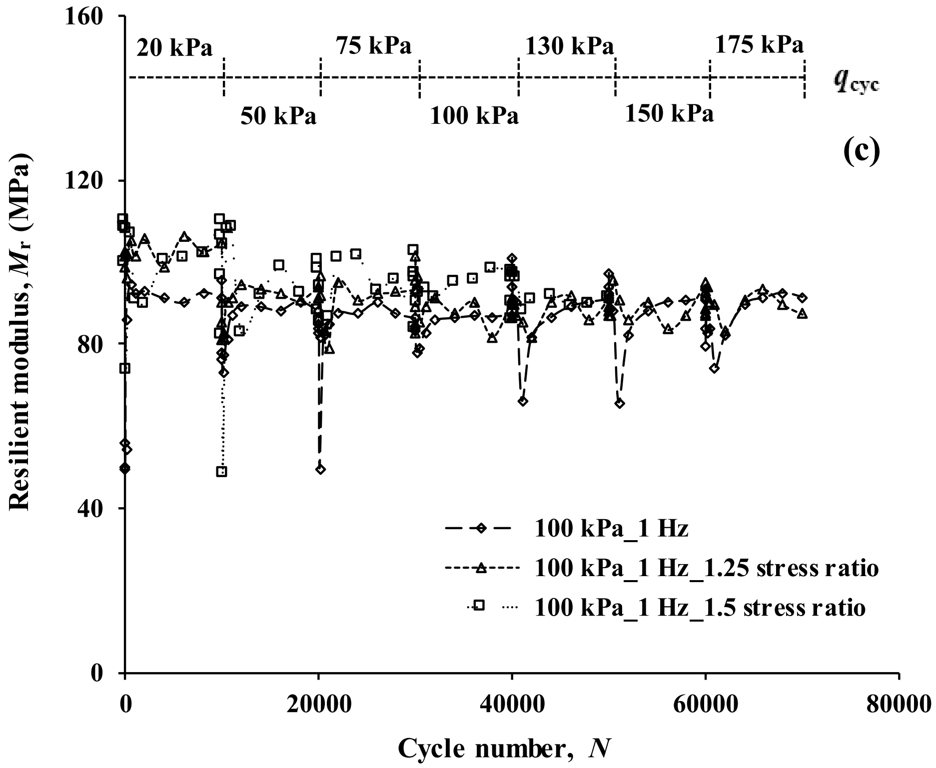

Figure 11. The plots of resilient modulus the specimens subjected to cyclic loading *versus* cycle number under (a) different initial effective confining pressures, (b) different frequencies, and (c) different consolidation stress ratios

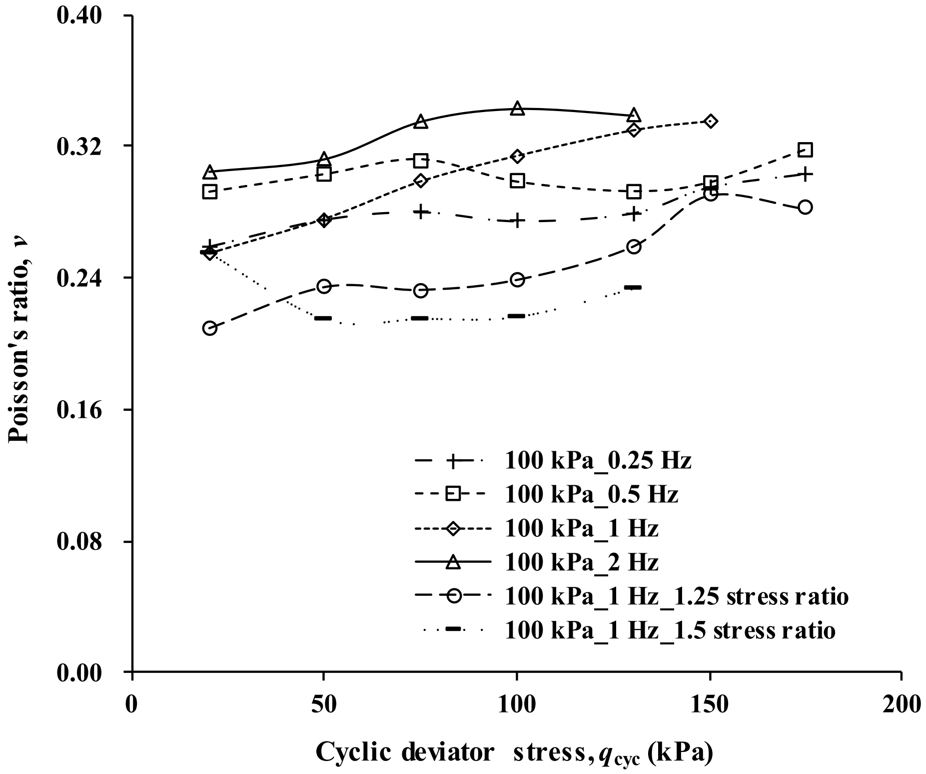

Figure 12. The plots of Poisson's ratio of the specimens under 100 kPa of initial effective confining pressure *versus* cyclic deviator stress

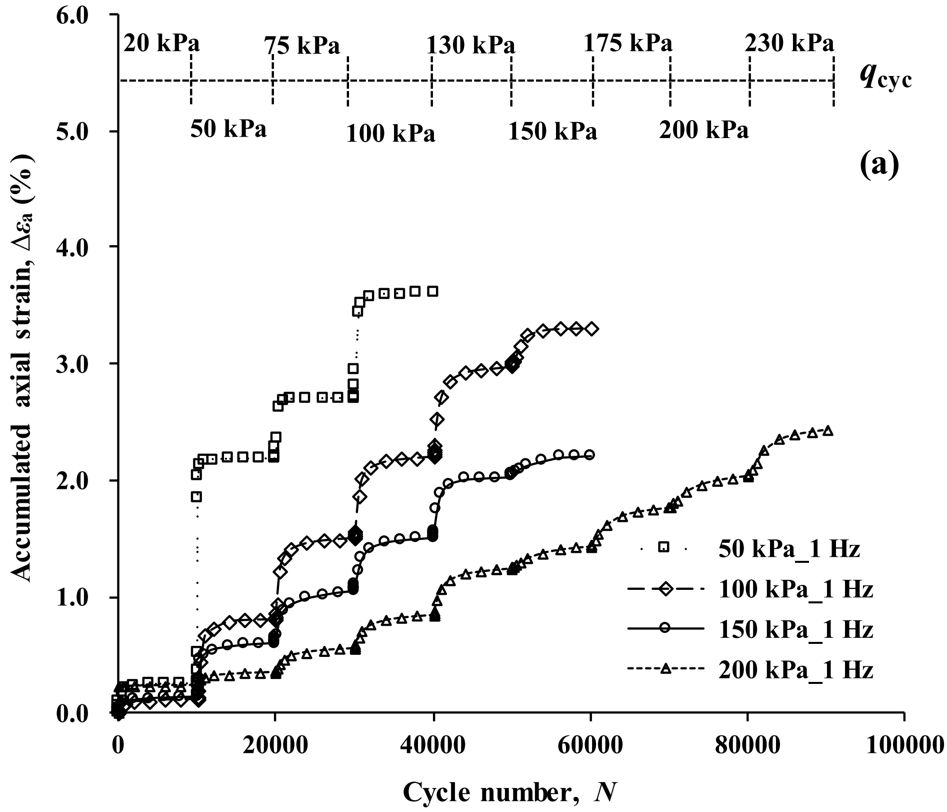

20 kPa
75 kPa
130 kPa
175 kPa
230 kPa
q_{cyc}
50 kPa
100 kPa
150 kPa
200 kPa
(a)
Accumulated axial strain, $\Delta\varepsilon_a$ (%)
50 kPa_1 Hz
100 kPa_1 Hz
150 kPa_1 Hz
200 kPa_1 Hz
Cycle number, N

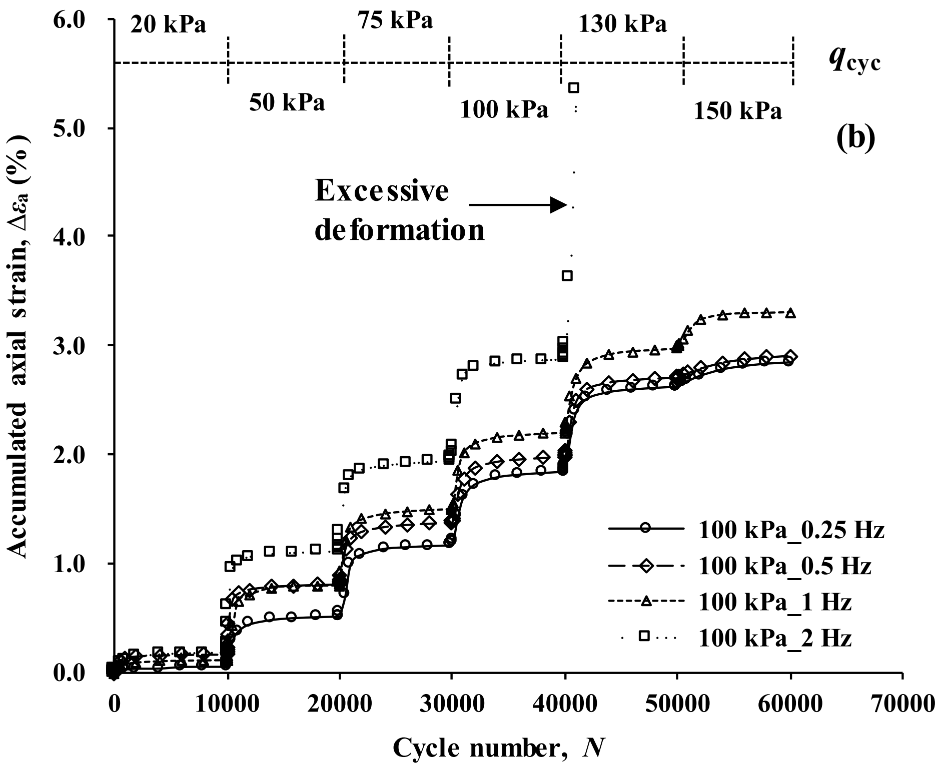

20 kPa
75 kPa
130 kPa
q_{cyc}
50 kPa
100 kPa
150 kPa
(b)
Excessive deformation
Accumulated axial strain, $\Delta\varepsilon_a$ (%)
100 kPa_0.25 Hz
100 kPa_0.5 Hz
100 kPa_1 Hz
100 kPa_2 Hz
Cycle number, N

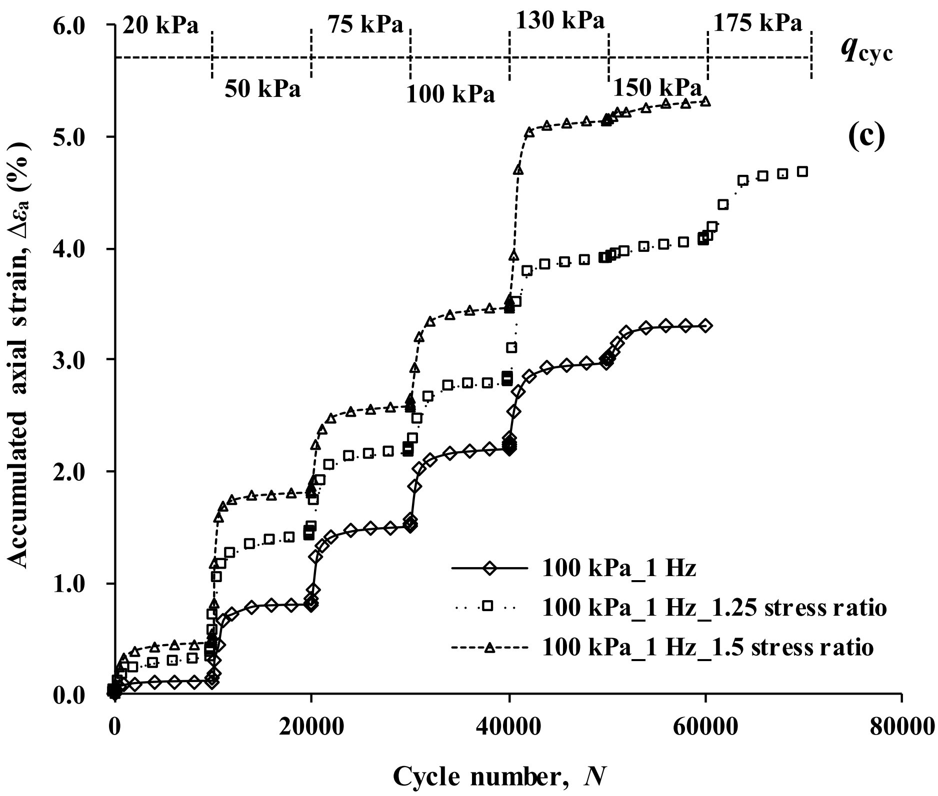

Figure 13. The plots of accumulated axial strains of the specimens subjected to cyclic loading *versus* cycle number under (a) different initial effective confining pressures, (b) different frequencies, and (c) different consolidation stress ratios

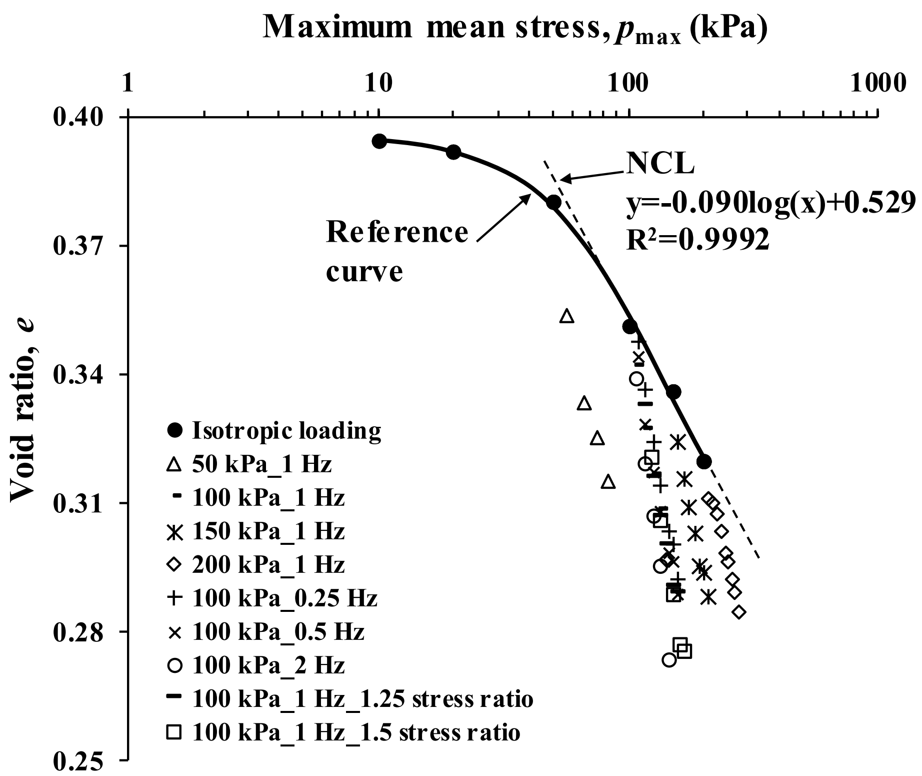

Figure 14. The relationship between the maximum mean stresses and the corresponding void ratios

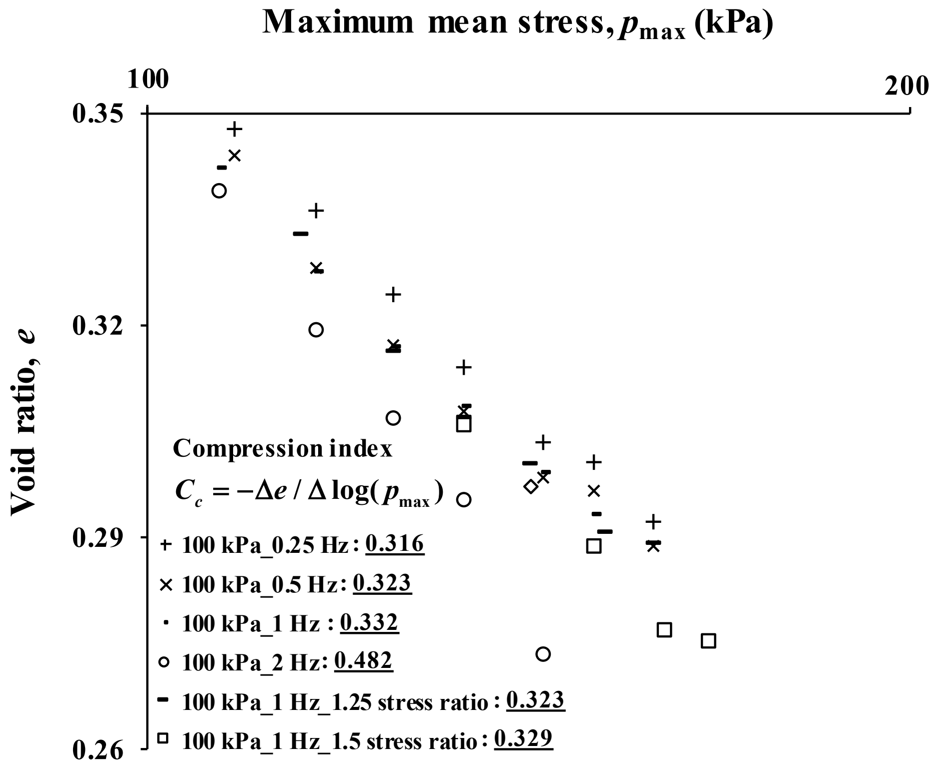

Figure 15. The relationship between the maximum mean stresses of the specimens consolidated by 100 kPa initial effective confining pressure and the corresponding void ratios

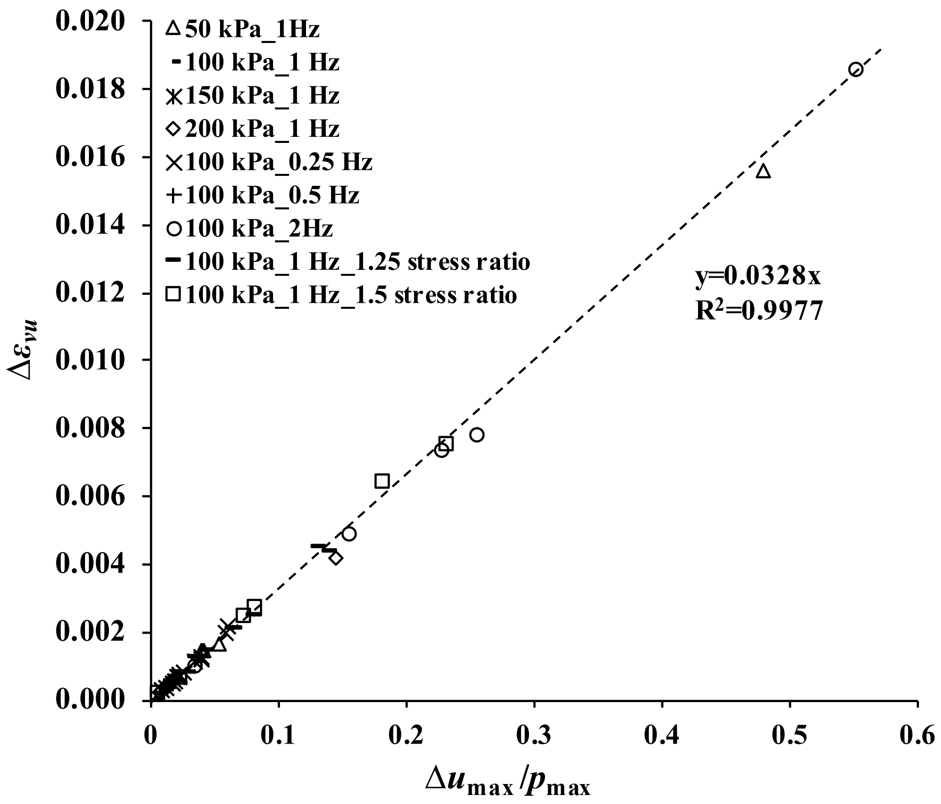

Figure 16. The relationship between volumetric strain due to disspation of excess pore water pressure ($\Delta\varepsilon_{vu}$) and $\Delta u_{\max}/p_{\max}$

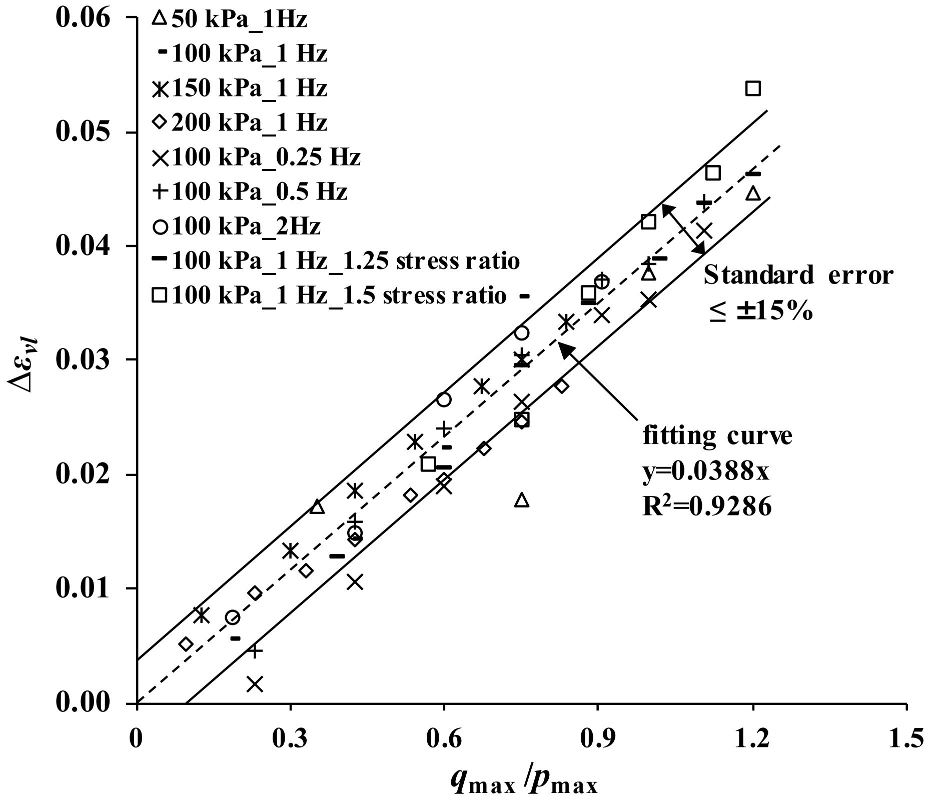

Figure 17. The relationship between the volumetric strain due to cyclic loading ($\Delta\varepsilon_{vl}$) and $q_{\max}/p_{\max}$

Table 1. Basic index values of tested granular fill material

Basic characteristics	**Value**
Coefficient of uniformity (C_u)	35.47
Coefficient of curvature (C_c)	0.138
Specific gravity (G_s)	2.73
Maximum dry density (MDD) ($\rho_{max,dry}$, kg/m^3)	2120.0
Optimum moisture content (OMC) (w_{opt}, %))	5.70

Table 2. XRF results of oxide content of tested granular fill material

Component	SiO_2	Al_2O_3	Fe_2O_3	MgO	K_2O	CaO
Content (%)	62.3	19.3	5.25	4.58	2.54	2.45

Table 3. Test scheme of tested granular fill material

Test No.	Initial effective confining pressure, σ'_3 (kPa)	Frequency, f (Hz)	Consolidation stress ratio, σ'_1/σ'_3	Cyclic deviator stress, q_{cyc} (kPa)	Remarks
50 kPa_static	50	-	-	-	Static compression
100 kPa_static	100	-	-	-	Static compression
200 kPa_static	200	-	-	-	Static compression
50 kPa_1 Hz	50	1	1	20, 50, 75, 100	With post-cyclic compression
100 kPa_0.25 Hz	100	0.25	1	20, 50, 75, 100, 130, 150, 175	-
100 kPa_0.5 Hz	100	0.5	1	20, 50, 75, 100, 130, 150, 175	-
100 kPa_1 Hz	100	1	1	20, 50, 75, 100, 130, 150, 175	With post-cyclic compression
100 kPa_2 Hz	100	2	1	20, 50, 75, 100, 130	-
100 kPa_1 Hz_1.25 stress ratio	100	1	1.25	20, 50, 75, 100, 130, 150, 175	-
100 kPa_1 Hz_1.5 stress ratio	100	1	1.5	20, 50, 75, 100, 130	-
150 kPa_1 Hz	150	1	1	20, 50, 75, 100, 130, 150, 175	-
200 kPa_1 Hz	200	1	1	20, 50, 75, 100, 130, 150, 175, 200, 230	With post-cyclic compression; permeability tests were conducted after each stage of isotropic loading and cyclic loading

Declaration of interests

√ The authors declare that they have no known competing financial interests or personal relationships that could have appeared to influence the work reported in this paper.

☐The authors declare the following financial interests/personal relationships which may be considered as potential competing interests: